 doi:10.20944/preprints202009.0287.v1

Article

Heating efficiency of $CoFe_{2-x}RE_xO_4$ (RE=Dy, Yb, Gd) magnetic nanoparticles for hyperthermia applications

Xanthippi Koutsoumbou[1], Ioannis Tsiaoussis[1], Georgiana Andreea Bulai[2], Ovidiu Florin Caltun[3]*, Orestis Kalogirou[1] and Charalampos Sarafidis[1]

[1] Department of Physics, Aristotle University of Thessaloniki, Thessaloniki, Greece;
[2] Integrated Centre for Environmental Science Studies in the North-East Development Region - CERNESIM, Alexandru Ioan Cuza University of Iasi, Iasi, Romania; georgiana.bulai@uaic.ro
[3] Laboratory of Magnetic Materials for Technological Applications – LMAT, Faculty of Physics, Alexandru Ioan Cuza University of Iasi, Iasi, Romania; caltun@uaic.ro

* Correspondence: caltun@uaic.ro; Tel.: 40740277065

Abstract: Cobalt ferrite nanoparticles (NPs) doped with rare earth (RE) metals with general formula $CoFe_{2-x}RE_xO_4$ (RE=Yb, Dy, Gd; x = 0.0 - 0.3) were synthesized by the co-precipitation method followed by post thermal treatment. The influence of RE doping on structural, magnetic and thermal properties and potential biomedical applications like magnetic hyperthermia has been investigated. In the as-prepared samples RE cations enter the spinel lattice as detected by X-ray diffraction. Thermal treatment leads to thermodynamically stable and relaxed single-phase spinel structures only for lower RE content, x = 0.01-0.05. However, annealed samples present higher mass magnetization values (M_S), up to 83 Am^2/kg. RE content also affects M_S, especially in the case of annealed samples where it decreases linearly with x from about 80 Am^2/kg (x = 0.01) to about 60 Am^2/kg (x = 0.30). Thermal treatment induces a reduction in coercivity from 60-100 mT for as-prepared samples to 18-33 mT for annealed samples, in a nonlinear manner with respect to RE content. Heating efficiency, i.e., Specific Loss Power (SLP), of all samples has been studied using both magnetometric and calorimetric method to deeper examine the energy loss mechanisms involved.

Keywords: rare earth doped cobalt ferrite nanoparticles; hyperthermia and heating efficiency

1. Introduction

Cobalt ferrite nanoparticles ($CoFe_2O_4$ NPs) have attracted a great interest for medical application over recent years, because they present useful properties such as thermal stability, mechanical hardness, high magnetocrystalline anisotropy (180 - 200 $kJ \cdot m^{-3}$) compared to Fe_3O_4 and larger coercivity combined with a moderate M_S (50 – 90 Am^2/kg) [1], [2]; even though some researchers have raised the toxicity issue [3–5]. These characteristics make $CoFe_2O_4$ NPs candidate materials for use in a wide range of applications (e.g. MRI contrast agents [6], DNA insulation [7], drug delivery [8], magnetic particle hyperthermia [9]) under the reserve of increasing biocompatibility [10,11]. In order to achieve the optimum thermal efficiency for magnetic hyperthermia applications it is important to understand how the magnetic field conditions and the properties of the MNPs could be fine-tuned.

The substitution of Fe^{3+} by Rare Earth (RE) cations may be used to tailor the magnetic properties of magnetic nanoparticles (MNPs) for hyperthermia-based applications [12]. Several research groups have synthesized RE doped cobalt ferrite materials [13–15] in both bulk and nanoparticle forms, by different methods such as solid-state reaction, solution combustion and co-precipitation; and have investigated their magnetic and structural properties [16–18]. These studies have shown that the magnetic and structural properties of RE doped ferrites depend on different parameters such as the

 doi:10.20944/preprints202009.0287.v1

RE dopant element and concentration, the synthesis method and subsequent processing. Hence, it is not known in advance what the effect of RE doping could be on the magnetic and structural parameters of ferrous oxide compounds. Magnetic behavior of ferrimagnetic oxides is mainly governed by 3d interactions; therefore, the incorporation of RE cations into the spinel structure and the resulting 4f-3d coupling may introduce changes in magnetization and Curie temperature. RE-RE interactions are also present but due to the indirect (4f-5d)-(5d-4f) character are considered weak [19].

Magnetic particle hyperthermia, i.e., the usage of magnetic nanoparticles (MNPs) as heating centers due to the interaction of their magnetic moments with an applied alternating magnetic field is a promising technique for various applications [20,21]. Fine-tuning of structural and magnetic properties of MNPs is critical for their heating performance [22,23]. In a previous study conducted by Virlan et al. [24] a series of RE-doped Co ferrite MNPs with nominal stoichiometry $CoFe_{2-x}RE_xO_4$ (RE = Yb, Dy, Gd; x = 0.01 - 0.3) have been obtained using the co-precipitation method and their specific absorption rate was studied using calorimetric methods. A large heat generating capability at an alternating field of 5 mT - 400 kHz was detected.

In the present work a similar series of samples both in as-prepared and thermal treated state is revisited in order to improve the understanding of the RE ions influence and particularly to study the effect of annealing on the structural and magnetic properties as well as on the thermal efficiency of $CoFe_{2-x}RE_xO_4$ (RE = Yb, Dy, Gd; x = 0.01 - 0.3) MNPs. Phase composition and structural parameters have been studied by Rietveld analysis of X-ray diffraction data; the extent of RE substitution that could be achieved in the spinel structure was investigated. Thermal efficiency was studied by using both the magnetometric approach as well as the calorimetric approach [24,27]; in the latter case an adiabatic approximation correction was applied in a similar scheme but with different field parameters compared to those reported in [24]. Magnetic hyperthermia measurements and minor hysteresis loops were utilized in order to compare Specific Loss Power (SLP) values of the samples with different dopant substitution and stoichiometry, before and after heat treatment. Determination and quantification of the factors which affect the SLP were calculated following a recently proposed scheme where most of the contributing factors and conditions have been standardized [27].

2. Materials and Methods

The as-prepared materials under study were synthesized by co-precipitation method as reported in detail by Virlan et al. [24]. Carboxymentyl cellulose (CMC) was used as natural surfactant in a similar scheme as the one presented in [29], where the appropriate concentrates of reactants were used to achieve the desired stoichiometry for each sample. For the needs of the present work, part of each sample was annealed at 1250°C for 12 h in ambient air in order to investigate the effect on the structural, magnetic and thermal properties. X-ray powder diffraction data acquired by a SIEMENS D500 X-ray diffractometer with Cu$K\alpha$ radiation in a Bragg-Brentano geometry were analyzed with the Rietveld method [30]. Crystallite size of the nanoparticles was estimated using Scherrer's equation for the five most intense peaks of the spinel ferrite phase. Additional structural and morphological properties were determined by High Resolution Transmission Electron Microscopy (HRTEM) micrographs using a 200 kV JEM-2011 microscope with an atomic resolution of 0.194 nm and by Scanning Electron Microscopy (SEM) using a JEOL JSM-840A apparatus coupled with an Oxford ISIS 300 microscope for energy dispersive X-ray spectroscopy (EDX). Thermogravimetric Analysis (TGA) was carried out in order to estimate the percentage of surfactant present on the nanoparticles surface using a SETA-RAM SetSys-1200 device. Magnetic characterization was performed using a PAR 155 Vibrating Sample Magnetometer (VSM) calibrated with a Ni reference sample. Thermal losses were calculated by minor loops (-25 to 25 mT and -70 to 70 mT) by the methodology described in [31] and also using the calorimetric method at two different combinations of magnetic field amplitudes and frequencies (25 mT-765 kHz using an Ambrell Easyheat generator of 1.2 kW and 70 mT-375 kHz using a Shuangping Ultrahigh Frequency Induction Heating Machine 4.5 kW) by applying an adiabatic approximation correction as in [32]. In order to extract a more accurate SLP value, the reference signal due to the solvent (distilled water)

Preprints (www.preprints.org) | NOT PEER-REVIEWED | Posted: 13 September 2020 doi:10.20944/preprints202009.0287.v1

was subtracted from the measurement data, while the thermal losses to the environment occurring during the experimental procedure were also considered in the SLP estimation. Heating efficiency of RE = Dy samples was measured using both magnetic field amplitude and frequency combinations while for the other samples only the former combination was used.

3. Results and discussion

3.1. Crystalline structure by X-Ray

In Figure 1 the X-ray diffraction patterns of all samples before and after annealing are presented. Unit cell parameters determined by Rietveld analysis as well as crystallite size determined by Scherrer's equation are summarized in Table I, including a reference sample of pure Co ferrite.

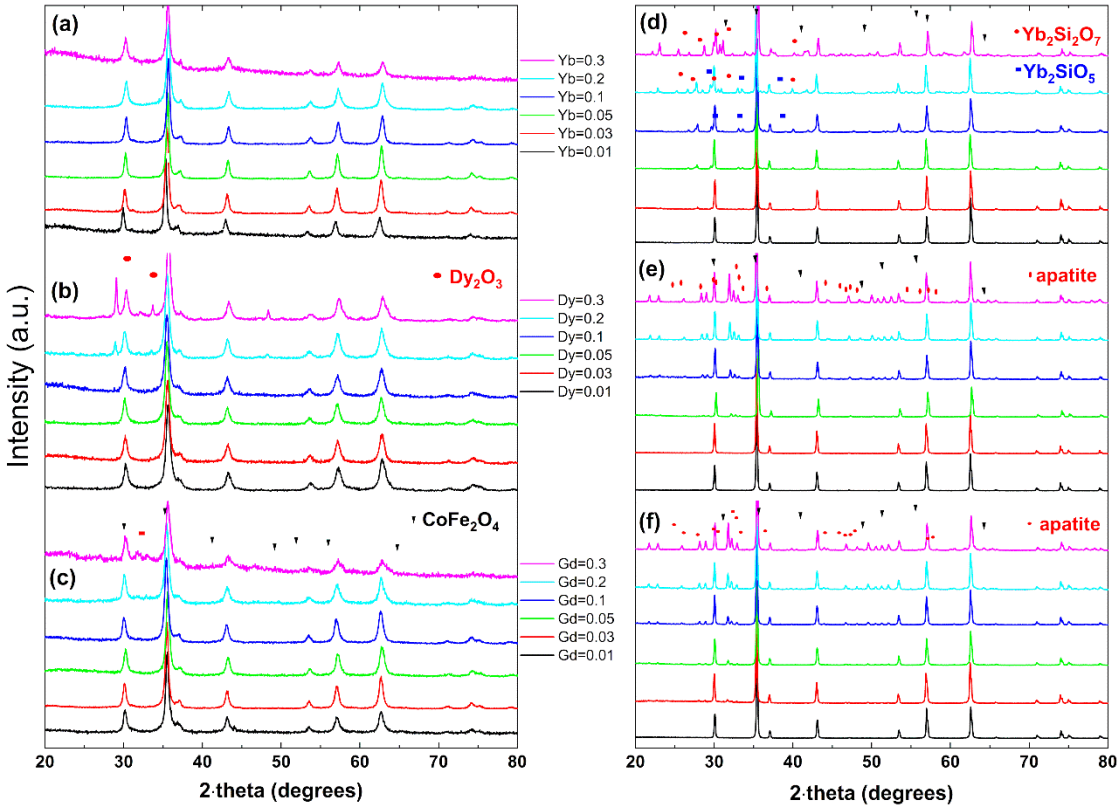

Figure 1. X-ray diffraction patterns of all the samples, not annealed RE = Yb (a), Dy (b), Gd (c) and annealed RE = Yb (d), Dy (e), Gd (f); x = 0.1 – 0.5.

Table 1. Structural properties of rare earth doped cobalt ferrite (RE = Yb, Dy, Gd; x = 0.1 – 0.5).

Compound	lattice parameter (nm)	unit cell volume ($nm^3\ x\ 10^3$)	Unit cell density (g/cm^3)	Crystallite size (nm)	(%wt.) of $CoFe_2O_4$	(%wt.) of secondary phases
$CoFe_2O_4$	0.8376(4)	587.7(4)	5.301	17.2	100	
$CoFe_{1.99}Dy_{0.01}O_4$	0.8357(4)	583.7(4)	5.338	13.3	100	
$CoFe_{1.97}Dy_{0.03}O_4$	0.8354(2)	583.1(2)	5.343	13.7	100	
$CoFe_{1.95}Dy_{0.05}O_4$	0.8361(4)	584.5(4)	5.331	14.9	100	
$CoFe_{1.9}Dy_{0.1}O_4$	0.8357(6)	583.7(6)	5.337	13.4	100	
$CoFe_{1.8}Dy_{0.2}O_4$	0.8353(6)	583.3(6)	5.341	13.8	97.1	2.9
$CoFe_{1.7}Dy_{0.3}O_4$	0.8354(6)	582.9(6)	5.344	13.2	92.2	7.8

 doi:10.20944/preprints202009.0287.v1

$CoFe_{1.99}Yb_{0.01}O_4$	0.8378(5)	588.2(6)	5.297	20.4	100	-
$CoFe_{1.97}Yb_{0.03}O_4$	0.8382(3)	589.0(4)	5.290	18.0	100	-
$CoFe_{1.95}Yb_{0.05}O_4$	0.8382(2)	588.8(3)	5.291	22.3	100	-
$CoFe_{1.9}Yb_{0.1}O_4$	0.8380(3)	588.4(4)	5.295	18.7	100	-
$CoFe_{1.8}Yb_{0.2}O_4$	0.8368(6)	586.0(8)	5.317	15.4	100	-
$CoFe_{1.7}Yb_{0.3}O_4$	0.8352(1)	583.0(1)	5.248	16.5	100	-
$CoFe_{1.99}Gd_{0.01}O_4$	0.8372(4)	586.8(3)	5.309	16.6	100	
$CoFe_{1.97}Gd_{0.03}O_4$	0.8373(3)	587.1(3)	5.307	18.3	100	
$CoFe_{1.95}Gd_{0.05}O_4$	0.8371(4)	586.6(5)	5.311	16.0	100	
$CoFe_{1.9}Gd_{0.1}O_4$	0.8370(4)	586.4(5)	5.313	16.1	100	
$CoFe_{1.8}Gd_{0.2}O_4$	0.8349(4)	582.0(6)	5.353	14.4	96.1	3.9
$CoFe_{1.7}Gd_{0.3}O_4$	0.8332(5)	578.5(6)	5.385	14.4	95.2	4.8
Annealed Compounds						
$CoFe_{1.99}Dy_{0.01}O_4$	0.8389(4)	590.5(5)	5.276	49.6	100	-
$CoFe_{1.97}Dy_{0.03}O_4$	0.8390(1)	590.6(1)	5.275	60.8	100	-
$CoFe_{1.95}Dy_{0.05}O_4$	0.8388(1)	590.2(1)	5.278	59.9	96.8	3.2
$CoFe_{1.9}Dy_{0.1}O_4$	0.8389(1)	590.4(1)	5.277	51.8	92.2	7.8
$CoFe_{1.8}Dy_{0.2}O_4$	0.8384(1)	589.3(1)	5.287	58.3	84.4	15.6
$CoFe_{1.7}Dy_{0.3}O_4$	0.8381(4)	588.8(1)	5.291	54.7	78.5	21.5
$CoFe_{1.99}Yb_{0.01}O_4$	0.8387(1)	590.0(1)	5.280	62.9	100	-
$CoFe_{1.97}Yb_{0.03}O_4$	0.8386(1)	589.8(1)	5.282	59.7	98.1	1.9
$CoFe_{1.95}Yb_{0.05}O_4$	0.8387(1)	590.0(1)	5.281	57.4	95.6	4.4
$CoFe_{1.9}Yb_{0.1}O_4$	0.8384(1)	589.2(1)	5.287	51.9	92.6	7.4
$CoFe_{1.8}Yb_{0.2}O_4$	0.8385(1)	589.5(1)	5.285	53.5	81.0	11.9 / 7.1
$CoFe_{1.7}Yb_{0.3}O_4$	0.8382(1)	588.9(1)	5.290	46.0	78.5	21.5
$CoFe_{1.99}Gd_{0.01}O_4$	0.8387(4)	589.9(1)	58.7	100.0	100	-
$CoFe_{1.97}Gd_{0.03}O_4$	0.8385(1)	589.6(1)	54.1	99.1	99.1	0.9
$CoFe_{1.95}Gd_{0.05}O_4$	0.8387(1)	590.0(1)	55.0	96.4	96.4	3.6
$CoFe_{1.9}Gd_{0.1}O_4$	0.8385(1)	589.5(1)	57.2	92.7	92.7	7.3
$CoFe_{1.8}Gd_{0.2}O_4$	0.8385(1)	589.5(1)	53.9	85.9	85.9	14.1
$CoFe_{1.7}Gd_{0.3}O_4$	0.8380(1)	588.5(1)	53.9	79.3	79.3	20.7

In Figure 2 the dependence of the lattice parameter (a) on the RE content is depicted for all samples.

Preprints (www.preprints.org) | NOT PEER-REVIEWED | Posted: 13 September 2020 doi:10.20944/preprints202009.0287.v1

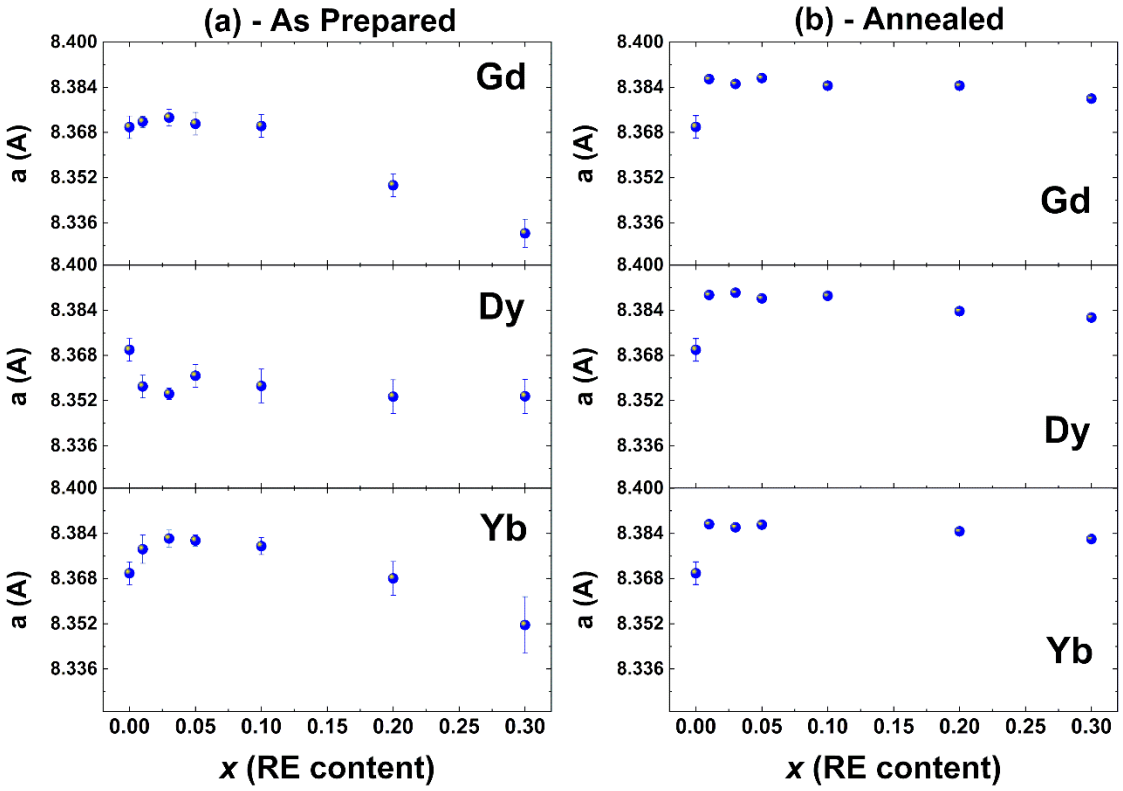

Figure 2. Lattice parameters of rare earth doped cobalt ferrite (RE = Yb, Dy, Gd; x = 0.1 – 0.5), not annealed (a) and annealed (b) samples

Almost all as prepared samples were found to be single phase, consisting only of the well-known fcc spinel-type structure of Co ferrite (S.G. No 227, F d -3 m). For the highest dopant concentrations (x = 0.2 and 0.3) and for RE = Dy and Gd small amounts of the respective RE_2O_3 oxides were detected. It is concluded that the formation of RE-doped Co ferrites is possible at least in a subspace of the specific stoichiometry range. The lattice parameter for the cases with RE = Yb, Gd expands slightly for low RE content up to 3% (x = 0.01 – 0.03). This observation can be attributed to the larger ionic radius of those RE atoms and their low concentration which in turn allows the accommodation of a small amount of RE atoms without significant distortion. For higher substitution concentration the lattice parameter drops almost linearly with a rate of about 0.2 Å for every 10% increase of the RE content, a result which is not profound. However, there are similar reports in the literature. Zhao et al. have observed similar behavior in Gd doped Co ferrites within a similar stoichiometry area [33]. Dixit et al. observed the same trend in RE doped Ni ferrite nanoparticles accompanied with reduction in crystallite size [34]. The same behavior is also evident in our case as seen in the data of Table I. These results are consistent with the fact that RE ions have a limited ability to replace Fe ones, due to their significantly increased size; the increasing difficulty for the RE ions to substitute Fe in the available octahedral positions distorts the unit cell. Excess RE atoms will eventually form secondary phases at the grain boundaries. Ahmed et al. have suggested a similar mechanism in RE substituted Mn-Zn ferrites [35]. For the case of RE = Dy there is no initial increase in lattice parameters. Actually, a large decrease is observed in lower RE content and then the subsequent decrease is less intense. This result is consistent with the proposed model and the small differences could be attributed to a combination of factors like ionic radius and RE-O binding energy. In our preliminary analysis factors like a) the energy variation which may be the result of the local structure relaxation, b) the chemical potential difference of the substitutional atom and the host structure and their possible anisotropic character are not taken into account since the necessary experimental techniques were not available, more work is required to fully understand this trend in unit cell parameters.

Preprints (www.preprints.org) | NOT PEER-REVIEWED | Posted: 13 September 2020 doi:10.20944/preprints202009.0287.v1

The X-ray diffraction patterns of the annealed samples present materials with improved crystallinity than their as-prepared counterparts (Figure 1(d)-(f)). This improvement, however, is accompanied with the appearance of secondary phases even at lower RE content. As the dopant concentration increases secondary phases gradually increase also, reaching 20 %wt. at the samples with the highest dopant concentration (x = 0.3) (Table I). These secondary phases include a $RE_{8.88}Si_{6.4}O_{26}$ apatite-type structure (SG No 176, P 63 / m) for RE = Dy, Gd while for Yb doped samples $Yb_2Si_2O_7$ (SG No 96, P 43 21 2) and Yb_2SiO_5 (SG No 15, I 1 2 /a 1) were identified. The presence of Si was confirmed in the EDX analysis and it probably originates in the equipment used for the calcination and annealing process. These phases have been observed in similar systems, e.g. [36-37]. In all cases of both annealed and not annealed samples these impurity phases do not present strong magnetic properties apart from a small dilution of the ferrite magnetization. Thermal treatment results in an increase in the lattice parameter for RE content up to 5%, compared to the as prepared counterparts. For 10% RE content and above lattice parameters remain almost constant. These results suggest that the percentage of rare earth content which can enter the spinel lattice, in order to form thermodynamically stable RE doped cobalt ferrites, is low and relatively constant, in the area of 1-5%. We assume that for this reason a small increase in lattice parameters with low RE contents occurred, as expected when the larger RE ions substitute the smaller Fe ions. Higher RE concentrations seem to lead to thermodynamically unstable cobalt ferrites, and for this reason, secondary phases were formed in the annealed samples.

3.2. Microstructure by SEM, TEM and EDX

Scanning Electron Microscope analysis of the samples was performed in order to investigate the morphology and chemical composition. Both as prepared and annealed samples were agglomerated, making difficult to study the size distribution of the NPs. Annealed nanoparticles presenting larger and more compact aggregates with irregular shapes and sharp edges. A typical example is presented in Figure 3. The presence of larger aggregates in annealed samples was attributed to the process of annealing and the burning of surfactant. The presence of surfactant in as-prepared NPs can be concluded from the morphology of their surface and the increased oxygen rates observed in most EDX spectra of these samples. The stoichiometric ratio of several spectra obtained from EDX analysis was close enough to the nominal stoichiometry of the main phase of the ferrite, typically less than ±5%, confirming its formation after taking into account the formation of secondary phases according to the results of Rietveld analysis of XRD plots.

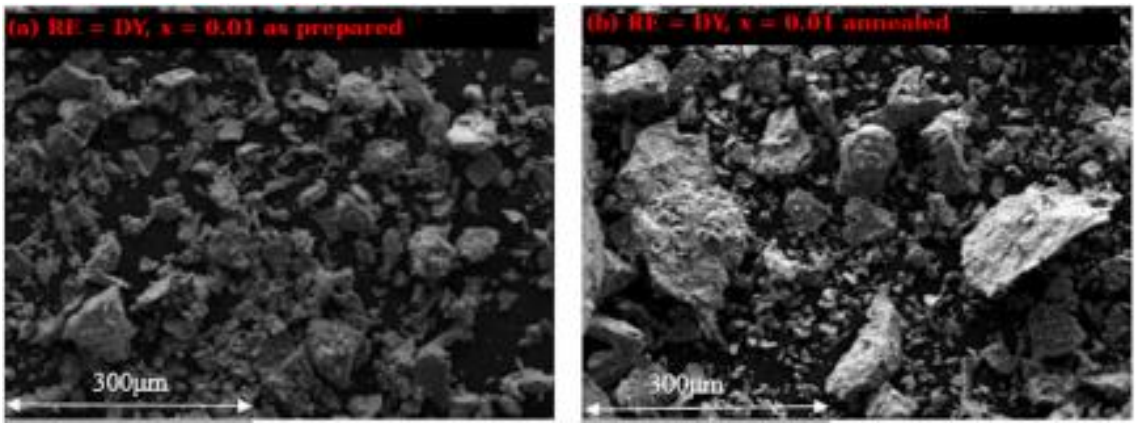

Figure 3. Typical microstructure in SEM for dysprosium doped samples as prepared (left – a) and annealed (right – b)

A more extensive structural and morphological characterization of the materials was performed by High Resolution Transmission Electron Microscopy (HRTEM) in order to investigate the size, shape, crystallites and d-spacing of annealed samples. These samples formed large aggregates and were precipitated in solutions, thus making difficult to obtain a large number of crystallites having

Preprints (www.preprints.org) | NOT PEER-REVIEWED | Posted: 13 September 2020 doi:10.20944/preprints202009.0287.v1

their lattice spacing perpendicular to the electron beam. An example where such crystallites could be distinguished can be seen in Figure 4(c).

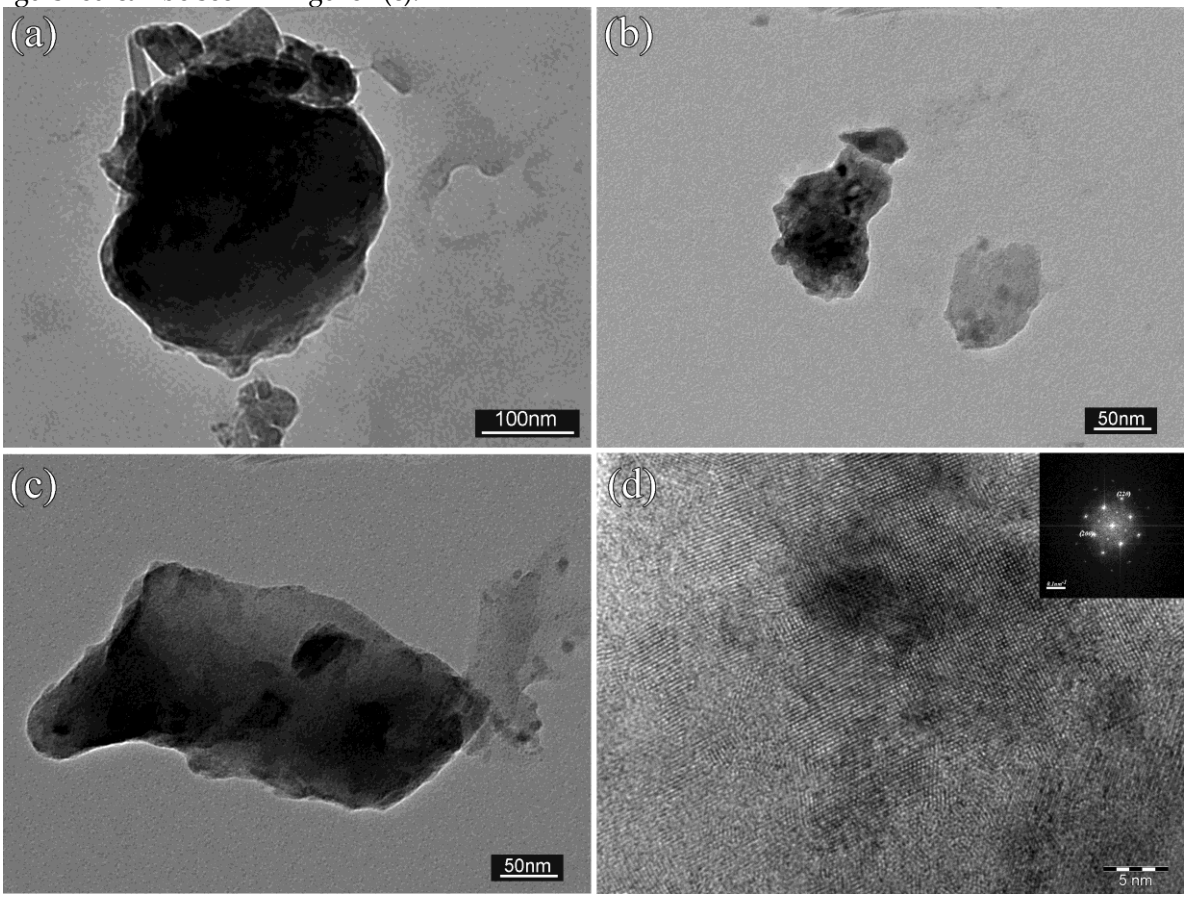

Figure 4. Typical TEM microstructure for annealed $CoFe_{1.95}Dy_{0.05}O_4$ particles; (a), (b) aggregates of 300 nm and 147 nm, respectively, (c) aggregate in which two crystallites measured 54 nm and 52 nm could be detected, (d) HRTEM micrograph with corresponding FFTs

Agglomerates were observed to have irregular shapes and large size and seem to be composed of many crystallites. The crystallite size values measured in those micrographs were close to the values estimated by Scherrer's equation for each sample. As it is seen in the HRTEM micrograph, a crystalline structure of about 35 nm is present (fig. 4(d)), where the d-spacings of the (200) planes as well as of the (220) planes are measured from the FFT image (inset), and it is found to be 0.421 nm and 0.296 nm respectively. The crystalline structure in the HRTEM micrograph seems to be dark on the left part of the image (Figure 4(d)). This could be explained either as due to the good orientation of the crystalline area with respect to the electron beam or as an indication of the presence of Dy at this area because of its larger atomic number Z. The d-spacing values confirmed the $CoFe_2O_4$ cubic structure but the RE ions lattice entrance cannot be absolutely confirmed. Using the contrast transfer function for the interpretation of the contrast variation at the distinct area or an STEM -EDS experiment could provide a better answer about the presence and possibly detection of the RE ions in atomic percentage in order to measure the lattice parameters.

3.3. Magnetic and hyperthermia properties

Major hysteresis loops of as prepared and annealed $CoFe_{1.95}RE_{0.05}O_4$ (RE=Dy, Yb, Gd) samples were recorded by vibrating sample magnetometry with ±2 T maximum applied field in order to investigate the basic magnetic properties of the materials. Prior to the measurements the instrument was calibrated against a Ni reference standard, M_S values are expected to have an accuracy within a 3% margin. Details for hyperthermia measurements accuracy are provided in [28]. The overall appearance of the loops is typical for MNPs of similar sizes [25]. In Fig. 5 the corresponding loops for the heat-treated samples are shown, with the part near the origins of the axes enhanced. The effect of

 doi:10.20944/preprints202009.0287.v1

stoichiometry in the basic magnetic properties can be observed. The decrease of M_S in all cases for $x > 0.05$ is evident. In Fig. 6 an indicative subset of major loops for as prepared samples of the same substitution are presented, including the reference material. The main observation is that RE doping enhances the M_S but this enhancement depends also on the type of the RE atom. In Fig. 7 a typical comparison of major loops for an as prepared and an annealed sample of the same composition (RE = Gd; $x = 0.5$) is presented, in order to observe the effect of thermal treatment in the loops. All the basic magnetic properties for the annealed samples are summarized in Table II, while mass magnetization versus RE content is plotted in Fig. 8. Thermal efficiency for the magnetometric method was calculated by multiplying each loop's area with the corresponding frequency of the calorimetric method, for the minor loops up to 25 mT this frequency was 765 kHz and for the minor loops up to 70 mT the frequency was 375 kHz; these frequencies were used in calorimetric experiments.

Preprints (www.preprints.org) | NOT PEER-REVIEWED | Posted: 13 September 2020 doi:10.20944/preprints202009.0287.v1

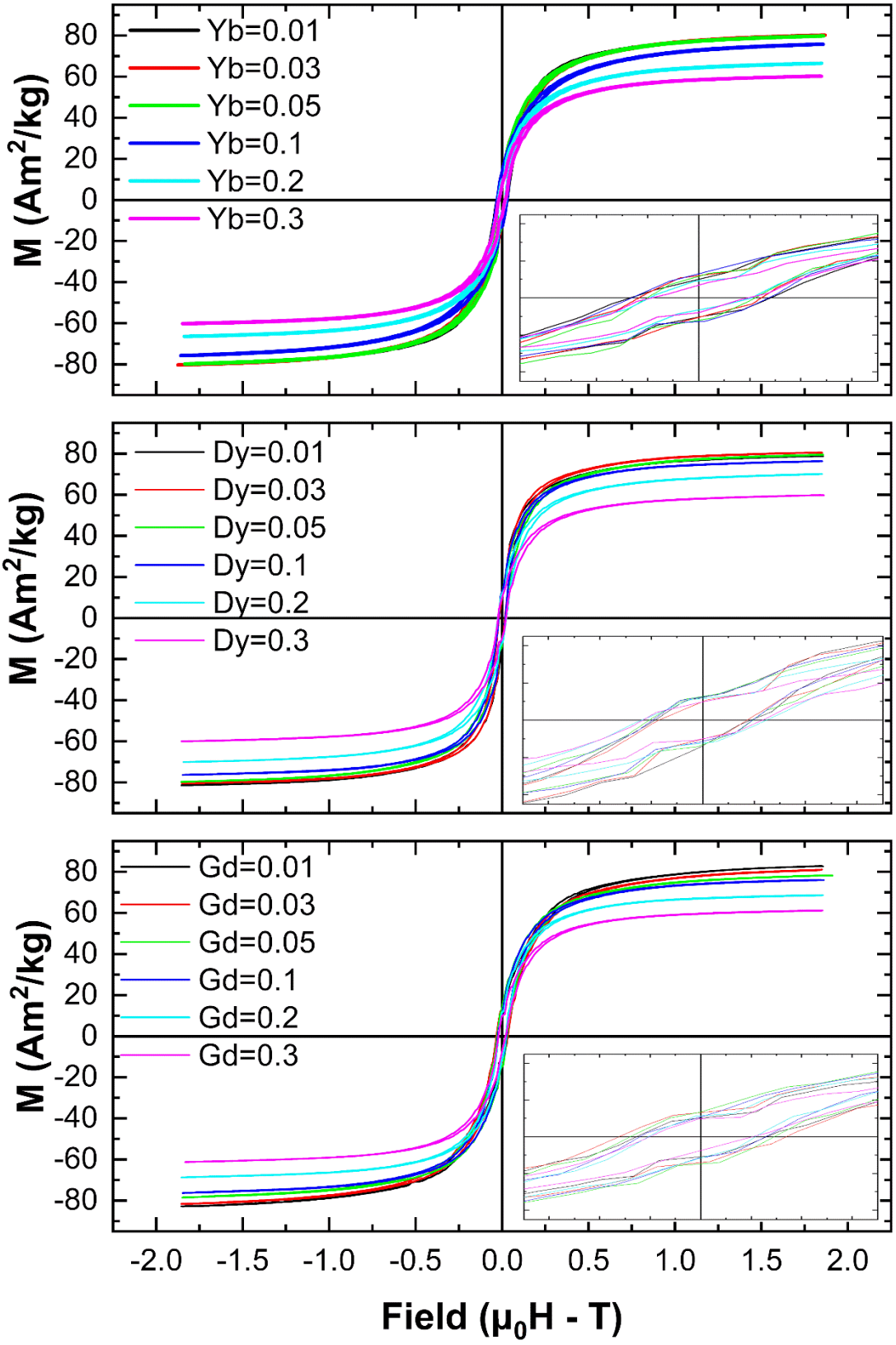

Figure 5. MHL curves for annealed $CoFe_{1-x}RE_xO_4$ samples grouped with the corresponding RE atom (top to bottom RE = Yb, Dy, Gd; x = 00.1 – 0.5). Coercive field is shown more clearly on the enlarged part of the loops in the inset

Preprints (www.preprints.org) | NOT PEER-REVIEWED | Posted: 13 September 2020 doi:10.20944/preprints202009.0287.v1

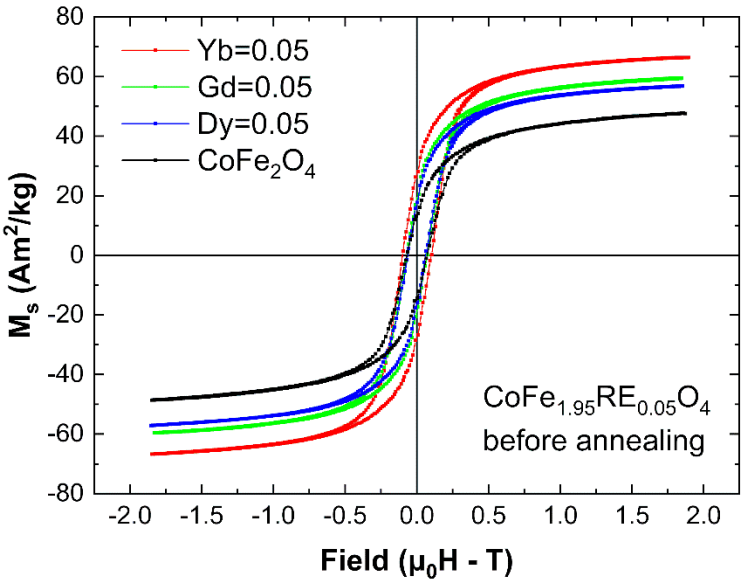

Figure 6. MHL curves for as prepared samples (RE = Yb, Dy, Gd; x = 0.05) and reference sample

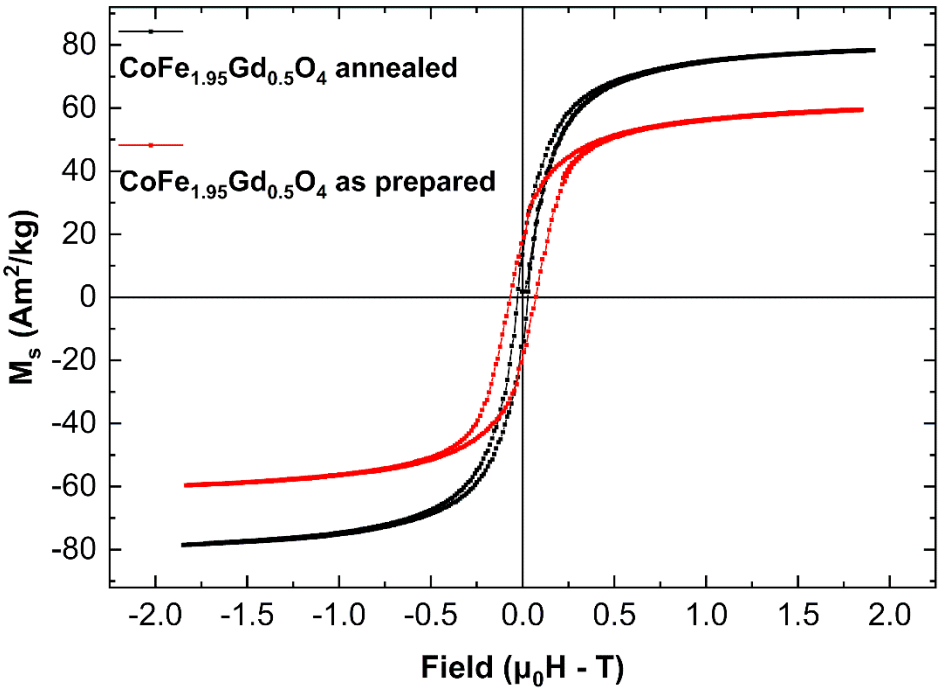

Figure 7. A comparison of MHL curves of as prepared and annealed samples (RE = Gd; x = 0.05)

Preprints (www.preprints.org) | NOT PEER-REVIEWED | Posted: 13 September 2020 doi:10.20944/preprints202009.0287.v1

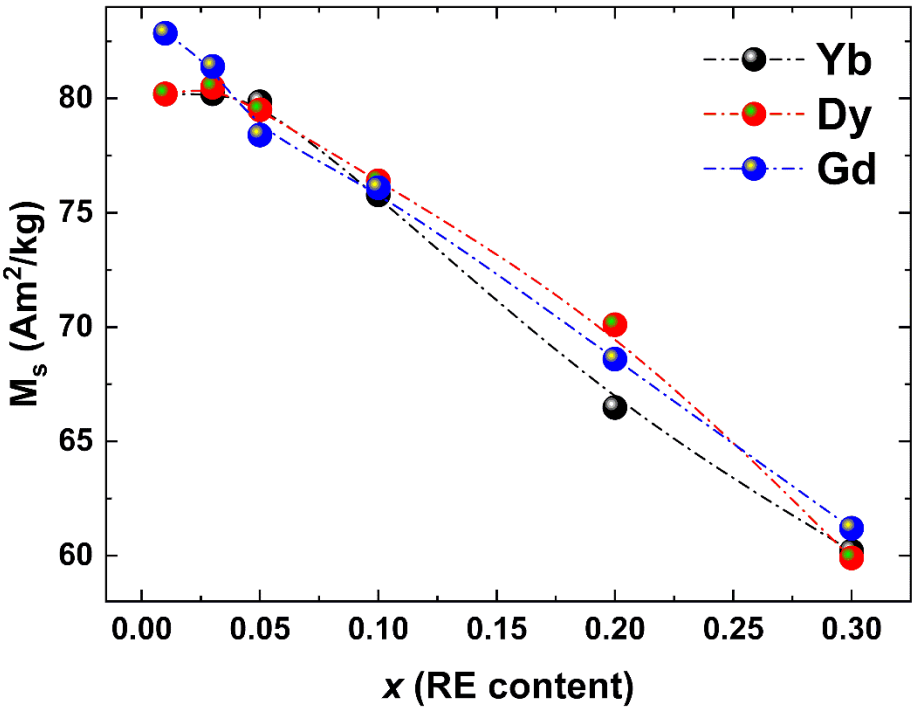

Figure 8. Mass magnetization versus RE content of annealed samples (RE = Yb, Dy, Gd; x = 0.1 – 0.5)

Table 2. Magnetic properties of $CoFe_{1-x}RE_xO_4$ annealed nanoparticles. Some values were not obtained due to apparatuses malfunction. SLP measurements at 70 mT are marked with an asterisk.

Compound (nominal)	Mass magnetization Ms (Am^2/kg)	Remanence (% of Ms)	Coercivity (μ_0H – mT)	SLP (W_H) estimation (25 mT / 70 mT*)	SLP calorimetric (25 mT / 70 mT*)
$CoFe_{1.99}Dy_{0.01}O_4$	80.2	17.2	19	500*	626/344*
$CoFe_{1.97}Dy_{0.03}O_4$	80.5	12.4	17	159/441*	491/219*
$CoFe_{1.95}Dy_{0.05}O_4$	79.5	16.4	20	136/511*	691/359*
$CoFe_{1.9}Dy_{0.1}O_4$	76.4	16.4	19	192/474*	610/341*
$CoFe_{1.8}Dy_{0.2}O_4$	70.1	16.3	24	437*	267/367*
$CoFe_{1.7}Dy_{0.3}O_4$	59.9	15.9	23	358*	151/264*
$CoFe_{1.99}Yb_{0.01}O_4$	80.1	13.1	27		199
$CoFe_{1.97}Yb_{0.03}O_4$	80.2	13.7	25	111	262
$CoFe_{1.95}Yb_{0.05}O_4$	79.9	14.4	22	121	378
$CoFe_{1.9}Yb_{0.1}O_4$	75.8	16.6	26	101	66
$CoFe_{1.8}Yb_{0.2}O_4$	66.5	13.4	20	108	39
$CoFe_{1.7}Yb_{0.3}O_4$	60.2	13.8	19	116	26
$CoFe_{1.99}Gd_{0.01}O_4$	82.9	13.9	25	77	79
$CoFe_{1.97}Gd_{0.03}O_4$	81.4	16.5	33		49
$CoFe_{1.95}Gd_{0.05}O_4$	78.4	17.2	28	89	199
$CoFe_{1.9}Gd_{0.1}O_4$	76.1	15.4	25		47
$CoFe_{1.8}Gd_{0.2}O_4$	68.6	17.2	22		87
$CoFe_{1.7}Gd_{0.3}O_4$	61.2	11.5	20	44	22

Mass magnetization of annealed RE doped samples was found in the range of 76-83 Am^2/kg for low RE contents (x=0.01-0.05), while for higher RE contents a decrease down to even 60 Am^2/kg is

 doi:10.20944/preprints202009.0287.v1

evident. The latter is attributed to the presence of the secondary phases. TG analysis was performed to estimate the percentage of surfactant present on the nanoparticles' surface. Weight loss of as-prepared samples ranged between 3-5 %, so it was assumed that the actual mass of nanoparticles used to calculate magnetization values was practically equal to their measured mass within the experimental error. Consequently, there is no significant error in data taken by VSM and hyperthermia measurements, with respect to the actual values of magnetic mass. In a previous work, mass magnetization values of as prepared RE doped Co ferrites were found to be lower, in the area of 50-60 Am^2/kg while coercivity was higher for the as prepared samples [24]; pure cobalt ferrite nanoparticles annealed at 1250 °C presented coercive field of 31.1 mT and magnetization of 73.6 emu/g at 1 T maximum applied field [15]. Our annealed nanoparticles have larger sizes, and this is consistent with our observations of their magnetic properties. It is known that coercive field reaches its maximum at the critical diameter in which nanoparticles converts from multi-domain to single domain, while magnetization decreases with the reduction of nanoparticles' size due to surface effects [38]. Critical diameter of Co ferrite has been reported to be in the range 50 to 70 nm [39]; however later studies suggest lower values from 23 to 40 nm [40–42]. It is reasonable to assume that other parameters that affect coercivity do not change significantly thus as-prepared samples were at the single domain region and therefore exhibited larger coercivity values than annealed samples, which could be considered as multi-domain nanoparticles.

For annealed samples, a linear decrease of saturation magnetization with the increase of RE content was observed. For the lowest dopant concentration, saturation magnetization was almost 80 emu/g, which is the value of Ms of the pure bulk cobalt ferrite. The reduction of saturation magnetization with the increase of RE content can be attributed to the non-magnetic secondary phases. In addition, even if the entire quantity of rare earth could enter the spinel lattice, both 3d-4f coupling and 4f-5d-4f coupling are weak interactions compared to Fe-Fe interactions which govern the magnetic response [19]. Coercivity of annealed samples presented a non-linear behavior with the increase of RE content, similarly to the behavior observed for as-prepared samples as reported in [24].

SLP values were calculated by utilizing magnetometric method on minor loops of several samples, with applied magnetic fields of 25 mT and 70 mT. A typical example depicting the differences between the two minor loops and the major loop of the as prepared sample is presented in Figure 9. SLP values from magnetometric method were estimated as described in [25,31].

Preprints (www.preprints.org) | NOT PEER-REVIEWED | Posted: 13 September 2020 doi:10.20944/preprints202009.0287.v1

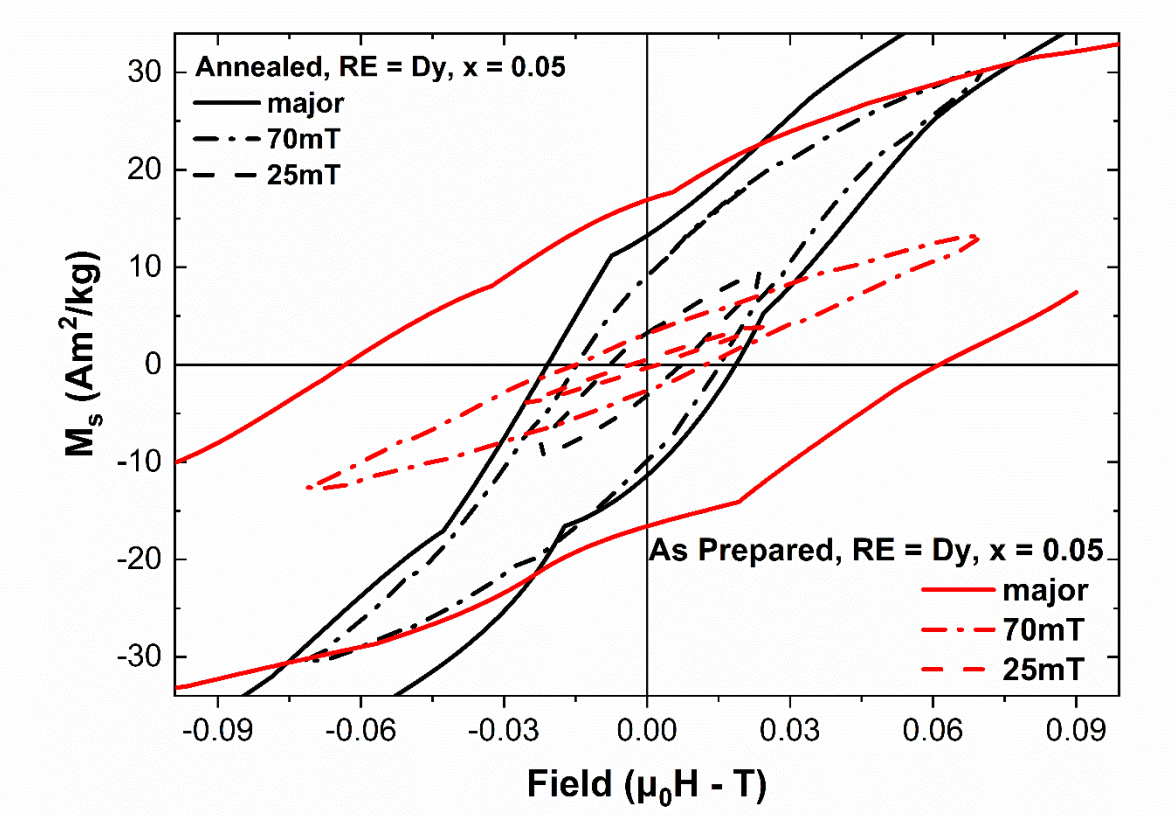

Figure 9. Typical differences between the two minor loops and the major loop (RE = Dy; x = 0.05)

It is worth noting that only an estimation of Specific Loss Power, as an order of magnitude, can be achieved by the magnetometric method due to the difference in experimental conditions compared to hyperthermia technique. Hysteresis losses were estimated by minor hysteresis loops and multiplied by the applied hyperthermia frequency, correspond to optimum power dissipation due to hysteresis losses. However, this comparison is mainly qualitative, since the estimation via a quasi-static magnetometry sequence is by virtue different from the actual behavior of the MNPs under the high frequency AC hyperthermia field. Additionally, in magnetometric method the samples are in the form of powder, under a static, non-alternating magnetic field, while in calorimetric method the samples are in suspensions under an alternating magnetic field. The results indicate higher thermal efficiency for annealed samples in comparison to as-prepared ones. Annealed samples exhibit higher saturation magnetization and lower coercivity as compared to the as prepared ones, due to size effect.

In the magnetometric method maximum thermal efficiency is obtained when the applied magnetic field for the minor loop is equal or larger than the coercivity of the samples. On the other hand, thermal efficiency is proportional to the hysteresis loop area of the samples. Annealed samples have lower coercivity and higher hysteresis loop areas than as prepared samples which means that lower magnetic field values are enough to achieve the maximum thermal efficiency these samples can give from the minor loops. It was also observed that estimated SLP values of Dy annealed samples were about eight times higher than as-prepared ones for 25 mT applied field, while only two times higher for 70 mT applied field (Figure 10(a)). Moreover, higher SLP values were estimated for Dy doped samples, for both as-prepared and annealed samples (Figure 10(b)) compared to the ones found for Yb and Gd doped samples with similar RE content.

Preprints (www.preprints.org) | NOT PEER-REVIEWED | Posted: 13 September 2020 doi:10.20944/preprints202009.0287.v1

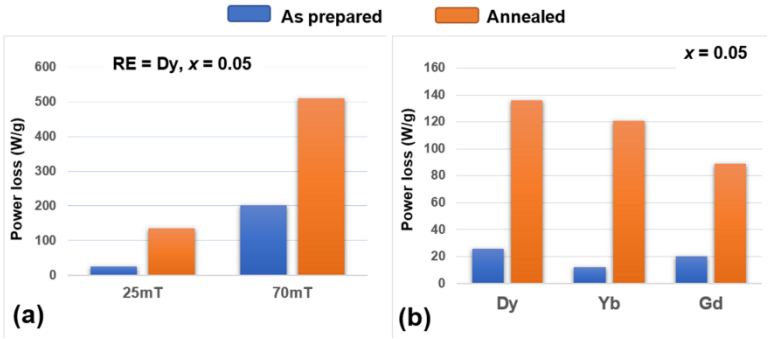

Figure 10. SLP values for as prepared and annealed doped samples; (a) RE = Dy; x = 0.05, (b) RE = Dy, Yb, Gd; x = 0.05, applied field 70 mT

Preprints (www.preprints.org) | NOT PEER-REVIEWED | Posted: 13 September 2020 doi:10.20944/preprints202009.0287.v1

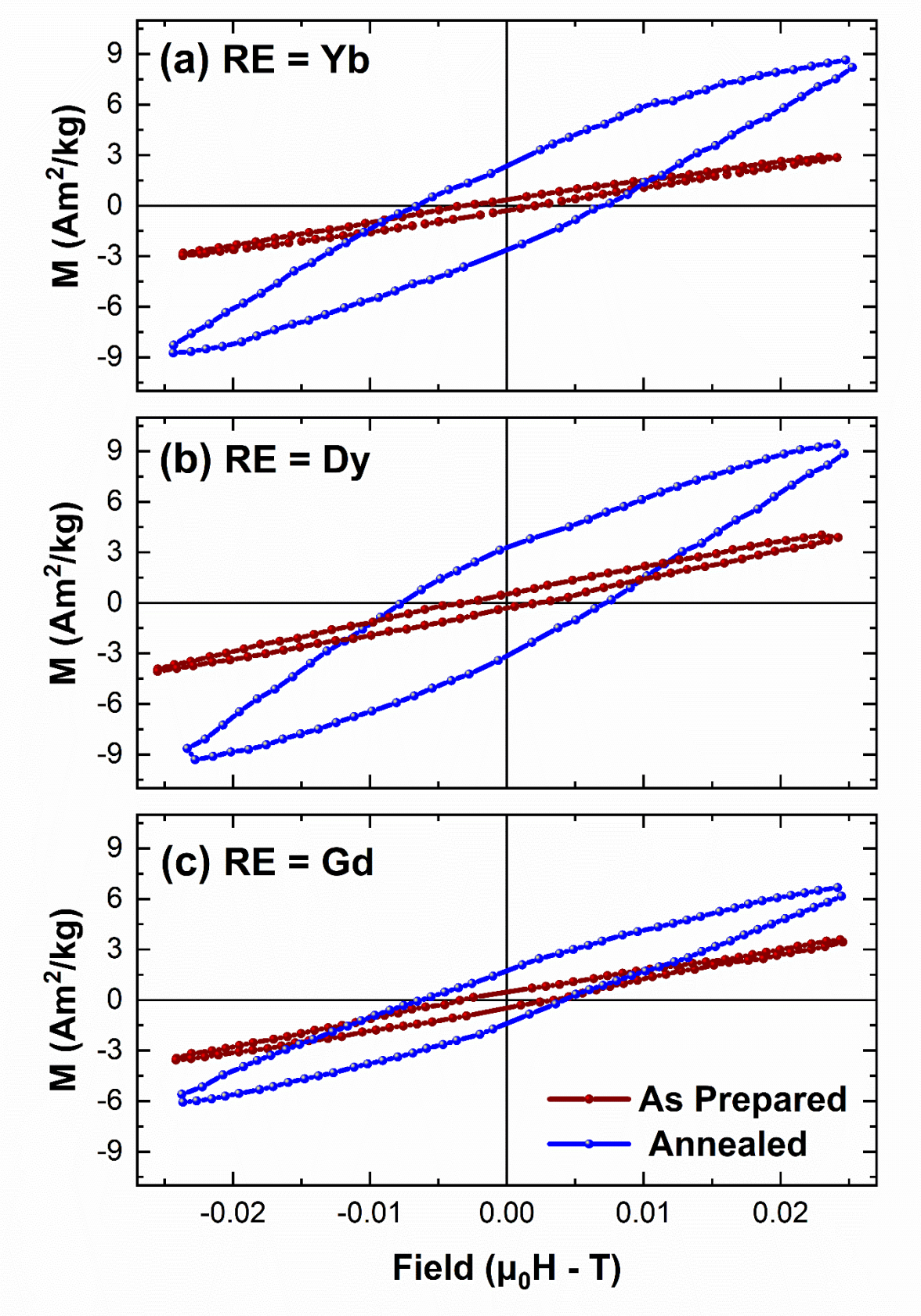

Figure 11. Minor MHL for as prepared and annealed samples (RE = Yb (a), Dy (b), Gd (c); x = 0.05)

In Fig. 11 minor hysteresis loops recorded at 25mT applied field ($\mu_0 H$) of as-prepared (red) and annealed (blue) $CoFe_{1.95}RE_{0.05}O_4$ samples for RE = Dy, Yb, Gd are presented, while in Fig. 12 a typical curve of SLP determination for the same material is depicted together with the heating curves of pure water for comparison.

Preprints (www.preprints.org) | NOT PEER-REVIEWED | Posted: 13 September 2020 doi:10.20944/preprints202009.0287.v1

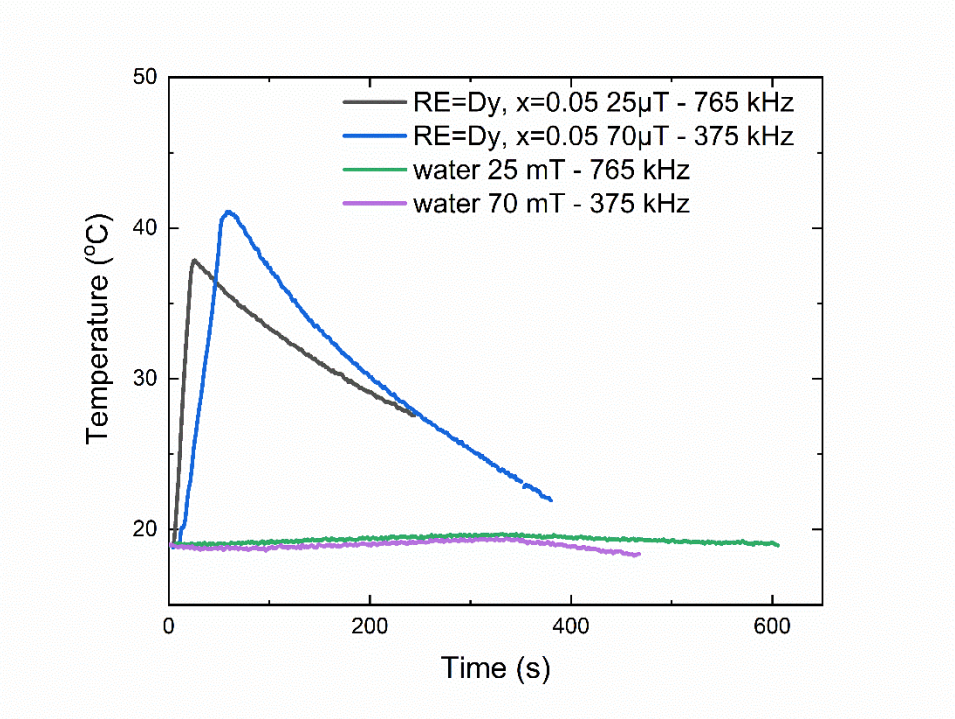

Figure 12. Heating curves for annealed $CoFe_{1-x}RE_xO_4$ samples (RE = Dy; x = 0.05) for both experimental conditions and respective pure water measurements.

SLP was also evaluated by the more reliable calorimetric method, under two different AC magnetic field parameters' set (25 mT-765 kHz for all samples, 70 mT-375 kHz for RE = Dy) by using Eq. 1 after applying an adiabatic correction as we have described above:

$$SLP = c\frac{m_f}{m_{Fe}}\frac{\Delta T}{\Delta t} \quad (1)$$

In Eq. 1 c is the specific heat of water (c = 4.185 J/g), mf the mass of water (1000 mg in our case), mFe the mass of magnetic powder (10 mg in our case) and ΔT/Δt the slope of temperature versus time of the adiabatic curve.

Hyperthermia results indicate that annealed samples presented higher SLP values than as-prepared samples. This could be explained by the larger loop area of annealed samples, as a result of their higher saturation magnetization values. However, the highest SLP values of annealed samples were obtained at the applied field of 25 mT and frequency of 765 kHz, with $CoFe_{1.95}Dy_{0.05}O_4$ exhibiting the maximum SLP value (691 ±138 W/g). In contrast, SLP values among as-prepared samples were in general higher at 70 mT-375 kHz reaching a maximum of approximately 60 ± 12 W/g, while at 25 mT-765 kHz their SLP was low. The above trend could be explained taking into consideration the results from magnetic measurements. Dy doped as-prepared samples exhibit coercivity values of 45-60 mT, while annealed ones of 17-25 mT. Applied field of 25 mT is enough to saturate the annealed samples' loops and hence is the higher frequency of 765 kHz which contributes to the achievement of higher SLP values. Moreover, annealed samples did not present colloidal stability and appeared to form aggregates in the form of chains during the experimental process. In the samples which presented those chain-shaped agglomerates, the temperature rise surged which was observed as an abrupt change in gradient of adiabatic curves. The suspensions of the samples, in which these large aggregates were observed, under the applied alternating field, presented higher SLP values. SLP seems to heavily depend on RE dopant, the higher SLP values were observed for Dy doped samples while the lowest for the case of RE = Gd. For the case of Dy doped samples we also observe a high sensitivity on RE content while in Yb doped materials is smaller and in the case of Gd doped materials is practically non-existing. There is hardly any

 doi:10.20944/preprints202009.0287.v1

correlation with the basic structural and magnetic properties of the materials, more work is needed in order to clarify this trend.

SLP values obtained via the two different methods were expected to be at the same order of magnitude. However, in the case where RE = Dy where we have obtained sufficient data, SLP values present some considerable differences. It is worth noting that only an estimation of SLP can be achieved by magnetometry, thus it was not expected to obtain directly comparable results between those two methods because of the differences in experimental conditions. In all cases of annealed samples, the calorimetric method produced higher SLP values. A possible explanation could be related to the formation of elongated clusters in the solution during the experiment and its induced additional anisotropy due to shape factor. We believe that more research is needed in this or similar systems in order to clarify this point.

4. Conclusions

RE doped Co ferrite MNPs with nominal stoichiometries $CoFe_{2-x}RE_xO_4$ (RE = Yb, Dy, Gd; x = 0.01 - 0.3) were successfully synthesized. RE atoms enter the spinel structure in all as prepared samples. Heat treatment produces thermodynamically relaxed materials with improved crystallinity which retain the spinel structure only for lower RE content; for large nominal RE amounts secondary phases are formed suggesting that the incorporation of the larger RE atoms in the system is limited. Doping with RE atoms enhance mass magnetization and coercivity in relation to pure Co ferrite, especially for the low RE compounds. However, thermal treatment reduces coercivity in a non-linear trend with respect to RE content due to the increase of the particles' size and the formation of the secondary phases. From the heat efficiency perspective, it is worth noting that both RE doping and the annealing process improve the thermal efficiency of the samples; all heat-treated compounds present higher SLP values. Larger nanoparticles (i.e. annealed ones) have better thermal response at 25 mT and 765 kHz compared to 70 mT and 375kHz (up to 89% increase of the maximum SLP value). The most important factor for heating efficiency is the type and the concentration of the RE dopant. Dy, in low concentration, showed the maximum improvement in SLP values combined with the most abrupt reduction with increasing dopant content. The underlying mechanism does not clearly correlates to the basic structural and magnetic properties.

Author Contributions: Conceptualization, Ovidiu Florin Caltun and Orestis Kalogirou; Data curation, Xanthippi Koutsoumbou, Iaris Tsiaoussis, Georgiana Andreea Bulai, Ovidiu Florin Caltun, Orestis Kalogirou and Charalampos Sarafidis; Investigation, Xanthippi Koutsoumbou, Iaris Tsiaoussis, Ovidiu Florin Caltun and Charalampos Sarafidis; Methodology, Ovidiu Florin Caltun, Orestis Kalogirou and Charalampos Sarafidis; Resources, Ovidiu Florin Caltun; Supervision, Ovidiu Florin Caltun; Writing – original draft, Iaris Tsiaoussis, Georgiana Andreea Bulai, Ovidiu Florin Caltun, Orestis Kalogirou and Charalampos Sarafidis; Writing – review & editing, Georgiana Andreea Bulai, Ovidiu Florin Caltun, Orestis Kalogirou and Charalampos Sarafidis.

Funding: "The publication as open access is funded by the Ministry of Research and Innovation within Program 1 – Development of the national RD system, Subprogram 1.2 – Institutional Performance – RDI excellence funding projects, Contract no.34PFE/19.10.2018.

Acknowledgments: Dr. M. Gjoka from the Institute of Nanoscience and Nanotechnology NCSR "Demokritos" is acknowledged for assisting on the XRD measurements of all samples. Dr. C. Virlan and Prof. dr. Aurel Pui for providing samples for hyperthermia measurements. Dr. A. Makridis from Department of Physics, AUTH is acknowledged for hyperthermia uncertainty calculations.

Conflicts of Interest: "The authors declare no conflict of interest.

References

1. Amiri, S. and Shokrollahi, H. The role of cobalt ferrite magnetic nanoparticles in medical science *Mater. Sci. Eng. C*, **2013** *33*, no. 1, pp. 1–8. DOI: 10.1016/j.msec.2012.09.003.
2. E. Demirci, E. Manna, P.K Wroczynskyj, Y. Aktürk, S. and van Lierop, J. Lanthanum ion substituted cobalt ferrite nanoparticles and their hyperthermia efficiency **2018** *J. Magn. Magn. Mater.*, *458*, pp. 253–260. DOI: 10.1016/j.jmmm.2018.03.024.
3. Kalia,S. Kango, S. Kumar, A. Haldorai, Y. Kumari, B. and Kumar, R. Magnetic polymer nanocomposites for environmental and biomedical applications *Colloid Polym. Sci.*, **2014** *292* no. 9, pp. 2025–2052. DOI: 10.1007/s00396-014-3357-y
4. Abudayyak, M Altincekic, T. Gurkaynak, T. and Özhan G. In Vitro Toxicological Assessment of Cobalt Ferrite Nanoparticles in Several Mammalian Cell Types *Biol. Trace Elem. Res.* **2017**, vol. 175, no. 2, pp. 458–465. DOI: 10.1007/s12011-016-0803-3
5. Aşik, E. Akpinar, Y. Tülin Güray, N. Işcan, M. Demircigil, G. Ç. and Volkan, M. Cellular uptake, genotoxicity and cytotoxicity of cobalt ferrite magnetic nanoparticles in human breast cells, Toxicol. Res. (Camb)., **2016** *5* no. 6, pp. 1649–1662. doi: 10.1039/c6tx00211k
6. Piché, D. Tavernaro, D. I. Fleddermann, J. Lozano, J. G. Varambhia, A. Maguire, M. L. Koch, M. Ukai, T. Hernández Rodríguez, A. J. Jones, L. Dillon, F. Reyes Molina, I. Mitzutani, M. González Dalmau, E. R. Maekawa, T. Nellist, P. D. Kraegeloh, A. Grobert, N. Targeted T 1 Magnetic Resonance Imaging Contrast Enhancement with Extraordinarily Small CoFe2O4 Nanoparticles *ACS Appl. Mater. Interfaces*, **2019** *11*, no. 7, pp. 6724–6740. doi.org/10.1021/acsami.8b17162
7. Rittich, B. Spanová, A. Horák, D. Benes, M. J. Klesnilová, L. Petrová, K. Rybnikár, A. Isolation of microbial DNA by newly designed magnetic particles *Colloids Surfaces B Biointerfaces* **2006** *52* no. 2, pp. 143–148. DOI: 10.1016/j.colsurfb.2006.04.012
8. Srinivasan, S. Y. Paknikar, K. M. Bodas, D. and Gajbhiye, V. Applications of cobalt ferrite nanoparticles in biomedical nanotechnology *Nanomedicine* **2018** *13*, no. 10, pp. 1221–1238. DOI: 10.2217/nnm-2017-0379
9. Nasrin, S. Chowdhury, F. U. Z. and Hoque, S. M. Study of hyperthermia temperature of manganese-substituted cobalt nano ferrites prepared by chemical co-precipitation method for biomedical application," *J. Magn. Magn. Mater.* **2019** *479* pp. 126–134. DOI: 10.1016/j.jmmm.2019.02.010.
10. Das, A. De, D. Ghosh, A. and Goswami, M. M. DNA engineered magnetically tuned cobalt ferrite for hyperthermia application *J. Magn. Magn. Mater.* **2019** *475* pp. 787–793. DOI: 10.1016/j.jmmm.2018.11.092.
11. Mushtaq, M. W. Kanwal, F. Batool, A. Jamil, T. Zia-ul-Haq, M. Ijaz, B. Huang Q. and Ullah, Z. Polymer-coated $CoFe_2O_4$ nanoassemblies as biocompatible magnetic nanocarriers for anticancer drug delivery *J. Mater. Sci.* **2017** *52* no. 16, pp. 9282–9293. DOI: 10.1007/s10853-017-1141-3.
12. Elayakumar, K. Dinesh, A. Manikandan, A. Palanivelu, M. Kavitha, G. Prakash, S. Thilak Kumar, R. Jaganathan, Saravana Kumar Baykall, A. Structural, morphological, enhanced magnetic properties and antibacterial bio-medical activity of rare earth element (REE) cerium (Ce^{3+}) doped $CoFe_2O_4$ nanoparticles," *J. Magn. Magn. Mater.* **2019** *476*, pp. 157–165. DOI: 10.1016/j.jmmm.2018.09.089
13. Cheng, F.-X. Jia, J.-T. Xu, Z.-G. Zhou, B. Liao, C.-S. and Yan, C.-H. Microstructure, magnetic, and magneto-optical properties of chemical synthesized Co-RE (RE-Ho, Er, Tm, Yb, Lu) ferrite nanocrystalline films *J. Appl. Phys.* **1999** *86*, no. 5, pp. 2727–2732. DOI: 10.1063/1.371117
14. Amiri S. and Shokrollahi, H. Magnetic and structural properties of RE doped Co-ferrite (RE=Nd, Eu, and Gd) nano-particles synthesized by co-precipitation *J. Magn. Magn. Mater.* **2013** *345* pp. 18–23. DOI: 10.1016/j.jmmm.2013.05.030.
15. Bulai, G. Diamandescu, L. Dumitru, I. Gurlui, S. Feder, M. and. Caltun, O. F. Effect of rare earth substitution in cobalt ferrite bulk materials," *J. Magn. Magn. Mater*. **2015** *390* pp. 123–131. DOI: 10.1016/j.jmmm.2015.04.089
16. Kambale, R. C. Song, K. M. Koo, Y. S. and Hur, N. Low temperature synthesis of nanocrystalline Dy^{3+} doped cobalt ferrite: Structural and magnetic properties *J. Appl. Phys.* **2011** *110* no. 5 p. 053910. doi.org/10.1063/1.3632987.
17. Dascalu, G. Popescu, T. Feder, M. and Caltun, O. F. Structural, electric and magnetic properties of $CoFe_{1.8}RE_{0.2}O_4$ (RE=Dy, Gd, La) bulk materials *J. Magn. Magn. Mater.* **2013** *333* pp. 69–74. DOI: 10.1016/j.jmmm.2012.12.048.
18. Rahman, M. T. Vargas, M. and Ramana, C. V. Structural characteristics, electrical conduction and dielectric properties of gadolinium substituted cobalt ferrite *J. Alloys Compd.* **2014** *617* pp. 547–562. DOI: 10.1016/j.jallcom.2014.07.182

19. Routray, K. L. Saha, S.. Sanyal, D. and Behera, D. Role of rare-earth (Nd^{3+}) ions on structural, dielectric, magnetic and Mossbauer properties of nano-sized $CoFe_2O_4$: Useful for high frequency application *Mater. Res. Express* **2019** *6* no. 2 026107 DOI: 10.1088/2053-1591/aaf2b5
20. Bahadur D. and Giri, J. Biomaterials and magnetism *Sadhana - Acad. Proc. Eng. Sci.* **2003** *28*, no. 3–4, pp. 639–656.
21. Dutz S. and Hergt, R. Magnetic particle hyperthermia - A promising tumour therapy? *Nanotechnology*, **2014** *25* no. 45, pp. 452001. DOI: 10.1088/0957-4484/25/45/452001
22. Pillai, V. and Shah, D. O. Synthesis of high-coercivity cobalt ferrite particles using water-in-oil microemulsions *J. Magn. Magn. Mater.* **1996** *163*, no. 1–2, pp. 243–248. DOI: 10.1016/S0304-8853(96)00280-6.
23. Shah, R. R. Davis, T. P. Glover, A. L. Nikles, D. E. and Brazel, C. S. Impact of magnetic field parameters and iron oxide nanoparticle properties on heat generation for use in magnetic hyperthermia *J. Magn. Magn. Mater.* **2015** *387* pp. 96–106, DOI: 10.1016/j.jmmm.2015.03.085.
24. Virlan, C. Bulai, G. Caltun, O. F. Hempelmann, R. and Pui, A. Rare earth metals' influence on the heat generating capability of cobalt ferrite nanoparticles *Ceram. Int.*, **2016** *42* no. 10, pp. 11958–11965. DOI: 10.1016/j.ceramint.2016.04.121
25. Zhao, L. Yang, H. Zhao, X. Yu, L. Cui, Y. and Feng, S. Magnetic properties of $CoFe_2O_4$ ferrite doped with rare earth ion *Mater. Lett.* **2006** *60* no. 1, pp. 1–6. DOI: 0.1016/j.matlet.2005.07.017.
26. Yamamoto, Y. Ogasawara, J. Himukai, H. and Itoh, T. Effects of coating molecules on the magnetic heating properties of Au-Fe_3O_4 heterodimer nanoparticles *Appl. Phys. Lett.* **2016** *109* no. 14, pp. 1–5. DOI: 10.1063/1.4964514
27. Doaga, A. Cojocariu, A. M. Amin, W. Heib, F. Bender, P. Hempelmann, R. Caltun, O. F. Synthesis and characterizations of manganese ferrites for hyperthermia applications *Mater. Chem. Phys.* **2013** *143* no. 1, pp. 305–310. DOI: 10.1016/j.matchemphys.2013.08.066
28. Makridis, A. Curto S., Van Rhoon, G. C. Samaras, T. and Angelakeris, M. A standardisation protocol for accurate evaluation of specific loss power in magnetic hyperthermia *J. Phys. D. Appl. Phys.* **2019** *52*, no. 25, pp. 255001 DOI: 10.1088/1361-6463/ab140c.
29. Gherca, D. Ciocarlan, R.-G. Cozma, D.-G. Cornei, N. Nica, V. Sandu, I. Pui, A. Influence of surfactant concentration (carboxymethylcellulose) on morphology and particle sizes of cobalt nanoferrites *Rev. Chim.* **2013** *64*, no. 8, pp. 848–851.
30. Hunter, B. A. Rietica-A visual Rietveld program *International Union of Crystallography Commission on Powder Diffraction Newsletter* **1998** No 20, p. 21.
31. V. Singh and V. Banerjee, "Ferromagnetism, hysteresis and enhanced heat dissipation in assemblies of superparamagnetic nanoparticles," J. Appl. Phys **2012** *112* no. 11 114912. DOI: 10.1063/1.4768904
32. Chalkidou, A. Simeonidis, K. Angelakeris, M. Samaras, T. Martinez-Boubeta, C. Balcells, L.l. Papazisis, K. Dendrinou-Samara, C. Kalogirou, O. In vitro application of Fe/MgO nanoparticles as magnetically mediated hyperthermia agents for cancer treatment *J. Magn. Magn. Mater. 323* **2011** no. 6 pp. 775–780. DOI: 10.1016/j.jmmm.2010.10.043
33. Zhao, X. Wang, W. Zhang, Y. Wu, S. Li, F. and Liu, J. P. Synthesis and characterization of gadolinium doped cobalt ferrite nanoparticles with enhanced adsorption capability for Congo Red *Chem. Eng. J.* **2014** *250* pp. 164–174.
34. Dixit, G. Pal Singh, J. Srivastava, R. C. and Agrawal, H. M. Magnetic resonance study of Ce and Gd doped $NiFe_2O_4$ nanoparticles *J. Magn. Magn. Mater.* **2012** *324* no. 4 pp. 479–483. DOI: 10.1016/j.jmmm.2011.08.027
35. Ahmed, M. A. Okasha, N. and El-Sayed, M. M. Enhancement of the physical properties of rare-earth-substituted Mn-Zn ferrites prepared by flash method *Ceram. Int.* **2007** *33* no. 1 pp. 49–58. DOI: 10.1016/j.ceramint.2005.07.014.
36. Mayer I. and Semadja, A. Magnetic effect studies of rare earth-containing apatites *J. Solid State Chem.* **1982** *43* no. 1 pp. 1–4. DOI: 10.1016/0022-4596(82)90208-0.
37. Singh R. K. and Srinivasan, A. Apatite-forming ability and magnetic properties of glass-ceramics containing zinc ferrite and calcium sodium phosphate phases *Mater. Sci. Eng. C*. **2010** *30* no. 8, pp. 1100–1106.
38. Jun, Y. W. Seo, J. W. and Cheon, J. Nanoscaling laws of magnetic nanoparticles and their applicabilities in biomedical sciences *Acc. Chem. Res.* **2008** *41* no. 2 pp. 179–189. DOI: 10.1021/ar700121f.
39. Berkowitz A. E. and Schuele, W. J. Magnetic Properties of Some Ferrite Micropowders *J. Appl. Phys.* **1959** *30* no. 4 pp. S134–S135. DOI: 10.1063/1.2185853.

40. Chinnasamy, C. N. Jeyadevan, B. Shinoda, K. Tohji, K. Djayaprawira, D. J. Takahashi, M. Justin Joseyphus, R. and Narayanasamy, A. Unusually high coercivity and critical single-domain size of nearly monodispersed $CoFe_2O_4$ nanoparticles *Appl. Phys. Lett.* **2003** *83* no. 14 pp. 2862–2864. DOI: 10.1063/1.1616655
41. K. Maaz, A. Mumtaz, S. K. Hasanain, and A. Ceylan, "Synthesis and magnetic properties of cobalt ferrite (CoFe2O4) nanoparticles prepared by wet chemical route," J. Magn. Magn. Mater., **2007** *308* no. 2, pp. 289–295. DOI: 10.1016/j.jmmm.2006.06.003.
42. Ramay S. M., Saleem, M. Atiq, S. Siddiqi, S. A. Naseem, S. and Sabieh Anwar, M. Influence of temperature on structural and magnetic properties of $Co_{0.5}Mn_{0.5}Fe_2O_4$ ferrites *Bull. Mater. Sci.* **2011** *34* no. 7 pp. 1415–1419. DOI: 10.1007/s12034-011-0337-4.